Title	Dynamic behavior of double-tapered-waveguide distributed feedback lasers
Author(s)	Yu, SF
Citation	IEEE Journal of Quantum Electronics, 1997, v. 33 n. 8, p. 1260-1267
Issued Date	1997
URL	http://hdl.handle.net/10722/42766
Rights	Creative Commons: Attribution 3.0 Hong Kong License

Dynamic Behavior of Double-Tapered-Waveguide Distributed Feedback Lasers

S. F. Yu

***Abstract*— Dynamic behavior of a double-tapered-waveguide (DTWG) distributed feedback (DFB) semiconductor laser is analyzed theoretically. It is found that the relaxation oscillation frequency can be enhanced by the DTWG structure especially for DFB lasers with large coupling-length product.**

***Index Terms*— Distributed feedback lasers, double-tapered waveguide, modeling, semiconductor lasers.**

I. Introduction

RECENTLY, double-tapered-waveguide (DTWG) distributed feedback (DFB) semiconductor lasers with buried heterostructure (BH) is proposed: 1) to reduce the influence of longitudinal spatial hole burning (SHB); 2) to maintain single-mode operation; 3) to minimize power density at facets; and 4) to reduce threshold current density [1], [2]. Extensive studies have verified that stable single-mode and high-power operation can be achieved in DTWG-DFB lasers with large coupling-length product $(\kappa L > 2.0)$ [2]. However, the relative important characteristics of DTWG-DFB lasers, the dynamic response under direct electrical modulation, has not been considered in their investigation.

In the rate-equation analysis, it has been shown that the square of relaxation oscillation frequency is directly proportional to the magnitude of lateral confinement factor [3]. Furthermore, the damping rate and relaxation oscillation period can be reduced significantly by the combined longitudinal and lateral effects especially for devices with strong lateral optical confinement and large coupling-length product $(kL > 2.0)$ [4]. This is due to the induced gain compression [5] and the nonuniform distribution of refractive index profile [6]. Therefore, it is expected that the relaxation oscillation frequency of DTWG-DFB lasers exhibits differently to the uniform waveguide DFB lasers. This is because: 1) the longitudinal distribution of lateral confinement factor as well as 2) the combined longitudinal and lateral SHB effects are dependent on the waveguide dimension (i.e., length and width of the tapered and phase-adjustment region) of DTWG-DFB lasers.

The above paragraph has explained that: 1) the longitudinal variation of lateral confinement factor; 2) the lateral SHB and carrier diffusion; and 3) the longitudinal SHB and refractive index distribution can have influence on the dynamic response of the DTWG-DFB lasers. However, in order to improve the dynamic behavior of the lasers, it is necessary to clarify their connection with the relaxation oscillation frequency of the devices and this forms the objective of this paper. In Section II, a self-consistent model including the combined longitudinal and lateral SHB effects as well as carrier diffusion is utilized to study the dynamic behavior of DTWG-DFB lasers. The spatial filtering effects of the tapered waveguide sections are also taken into account by using the effective index method [7]. Using the steady-state approximation, relaxation oscillation frequency of DTWG-DFB lasers is derived analytically. In Section III, the influence of double-tapered geometry on the modulation response of DFB lasers is studied numerically. Finally, a brief conclusion is given in Section IV.

Manuscript received December 16, 1996; revised April 10, 1997. This work was supported by HKU CRCG.

The author is with the Department of Electrical and Electronic Engineering, University of Hong Kong, Pokfulam Road, Hong Kong.

Publisher Item Identifier S 0018-9197(97)05434-1.

II. Numerical and Analytical Analysis of DTWG-DFB Lasers

A. Numerical Model of DTWG-DFB Lasers

The propagation of forward and reverse fields, $F(z,t)$ and $R(z,t)$, along the laser cavity with tapered waveguide can be described by the modified coupled wave equations as follows:

$$\left(\frac{1}{v_g}\frac{\partial}{\partial t} \pm \frac{\partial}{\partial z}\right)\begin{bmatrix}F\\R\end{bmatrix} = \left[\frac{1}{2}(\Gamma_x g(z,t) - \alpha_s) + i\delta\beta(z,t)\right] \times \begin{bmatrix}F\\R\end{bmatrix} + i\kappa(z)\begin{bmatrix}R\\F\end{bmatrix} \quad (1)$$

where v_g is the group velocity, Γ_x is the transverse confinement factor, and κ is the longitudinal coupling coefficient. α_s is the absorption and scattering loss in the waveguide and is assumed uniformly distributed along the lateral direction. g is the field gain given by

$$g(z,t) = \int_{\text{active}} a_N(N(y,z,t) - N_o)\psi_o^2(y)\, dy \quad (2)$$

where N is the carrier concentration distribution in the lateral and longitudinal directions, a_N is the differential gain, and ψ_o is the lateral field distribution. The deviation from the Bragg condition $\delta\beta$ is given as

$$\delta\beta(z,t) = \frac{2\pi}{\lambda_o} n_{\text{eff}}(z,t) - \frac{\pi}{\Lambda} \quad (3)$$

where c is the speed of light and Λ is the pitch of the grating. n_{eff} is the effective refractive index in the longitudinal direction. The change of effective refractive index can be calculated by using the method given in [7] and [8].

The time-dependent rate equation of carrier concentration is given by

$$\frac{dN(y,z,t)}{dt} = \frac{J(y,z,t)}{qd} - \frac{N(y,z,t)}{\tau} - v_g a_N \times (N(y,z,t) - N_o)\mathbf{P}(y,z,t) + D_f \frac{\partial^2 N(y,z,t)}{\partial y^2} \quad (4)$$

where J is the injection current density profile, d is the thickness of the active layer, D_f is the diffusion constant, τ is the carrier lifetime, and q is the electron charge. The photon density distribution $\mathbf{P}$ is given as

$$\mathbf{P}(y,z,t) = \left[|F(z,t)|^2 + |R(z,t)|^2\right]\psi_o^2(y) = P(z,t)\psi_o^2(y). \quad (5)$$

To simplify our calculation, the inhomogeneous carrier distribution in the lateral direction is expanded in a Fourier series. The first-order approximation of carrier distribution is then given by [9]

$$N(y,z,t) = N_p(z,t) - N_1(z,t)\cos(2\pi y/w) \quad (6)$$

where w is the width of the waveguide, N_p is the average carrier distribution in the longitudinal direction, and N_1 is the perturbation of carrier concentration in the lateral direction. Substituting (6) into (2) and (4), with J assumed constant across the active layer and integrating (2) and (4) over the active layer, including the gain compression coefficient ε, we obtain the modified field gain expression given as

$$g(z,t) = \frac{a_N\{\Gamma_y(z)(N_p(z,t) - N_o) - \xi_1(z)N_1(z,t)\}}{(1+\varepsilon P(z,t))} \quad (7a)$$

and the rate equations of carrier densities given as

$$\frac{dN_p(z,t)}{dt} = \frac{J(z,t)}{qd} - \frac{N_p(z,t)}{\tau} - \frac{v_g a_N\{\Gamma_y(z)(N_p(z,t)-N_o)-\xi_1(z)N_1(z,t)\}}{(1+\varepsilon P(z,t))} \times P(z,t) \quad (7b)$$

$$\frac{dN_1(z,t)}{dt} = \frac{2v_g a_N\{\xi_1(z)(N_p(z,t)-N_o)-\xi_2(z)N_1(z,t)\}}{(1+\varepsilon P(z,t))} \times P(z,t) - \frac{1+\gamma}{\tau}N_1(z,t) \quad (7c)$$

where Γ_y is the confinement factor in the lateral direction and ξ_1 and ξ_2 are the first- and second-order coupling parameters of the carriers and the optical field ψ_o. Their definitions are given in Appendix A. The parameter γ is given by

$$\gamma = 4\pi^2\tau D_f/w^2. \quad (8)$$

A self-consistent large-signal calculation can be obtained by solving (1) and (7) simultaneously.

It must be noted that the round-trip conditions of DTWG-DFB lasers are affected by their waveguide dimension. This is because the longitudinal propagation constant is changed according to the stripe width of waveguide, such that the deviation in propagation constant from Bragg constant is also dependent on the waveguide dimension. Therefore, the values of Γ_y, κ, $\delta\beta$, ξ_1, and ξ_2 are dependent on the stripe width of the waveguide and can be evaluated by the effective index method [7]. Detailed calculation of these parameters can be found in Appendix A.

B. Relaxation Oscillation Frequency of DTWG-DFB Lasers: Analytical Analysis

It is believed that the lateral and longitudinal effects (including waveguide structure and SHB profile) will have effect on the relaxation oscillation frequency of DTWG-DFB lasers. In order to investigate the influence of lateral and longitudinal effects, the analytical expression of relaxation oscillation frequency is derived from the time-dependent rate equations of photon density and carrier concentration. Therefore, the requirement for the enhancement of relaxation oscillation frequency of DTWG-DFB lasers can be clarified.

The derivation is started from the coupled wave equations. The rate equation of photon density can be deduced by multiplying (1) with its complex conjugate of the forward and reverse propagation fields and adding the two equations and their conjugates to obtain

$$\frac{\partial P}{\partial t} = (\Gamma_x(\Gamma_y G_P(N_P) - v_g a_N \xi_1 N_1) - v_g\alpha_p)P \quad (9)$$

where $P = |F|^2 + |R|^2$, $\alpha_p = \alpha_s + (\partial|F|^2 + |R|^2/\partial z)/(|F|^2 + |R|^2)$ and $G_P(N_P) = v_g a_N(N_P - N_o)$.

Rewriting (7b) and (7c) in terms of $G_p(N_P)$, we obtain

$$\frac{dN_p}{dt} = \frac{J}{qd} - \frac{N_p}{\tau} - \{\Gamma_y G_P(N_P) - v_g a_N \xi_1 N_1\}P \quad (10)$$

$$\frac{dN_1}{dt} = 2\{\xi_1 G_P(N_P) - v_g a_N \xi_2 N_1\}P - \frac{1+\gamma}{\tau}N_1. \quad (11)$$

In the derivation of (9)–(11), gain compression has been ignored. In (11), if the frequency of the modulation signal is less than the effective electron lifetime $\tau/(1+\gamma)$, it is possible to obtain an approximate solution to N_1 by setting the derivative to zero [9]. We have

$$N_1(z,t) = \tau'\xi_1 G_P(N_P)P/(1+\varepsilon_2 P) \approx \tau'\xi_1 G_P(N_P)(1-\varepsilon_2 P)P \quad (12)$$

where $\tau' = 2\tau/(1+\gamma)$ and $\varepsilon_2 = \tau' v_g a_N \xi_2$. The rate equations can be simplified by substituting (12) into (9) and (10). We have

$$\frac{\partial P}{\partial t} = \left(\Gamma_x\Gamma_y G_P(N_P)\left(1 - \left(\varepsilon_1^2/\Gamma_y\right)P + \left(\varepsilon_1^2\varepsilon_2/\Gamma_y\right)P^2\right) - v_g\alpha_p\right)P \quad (13a)$$

$$\frac{dN_p}{dt} = \frac{J}{qd} - \frac{N_p}{\tau} - \Gamma_y G_P(N_P)\left(1 - \left(\varepsilon_1^2/\Gamma_y\right)P + \left(\varepsilon_1^2\varepsilon_2/\Gamma_y\right)P^2\right)P \quad (13b)$$

where $\varepsilon_1^2 = \tau' v_g a_N \xi_1^2$. ε_1 and ε_2 can be considered to be the effective gain compression factors arisen from the lateral effects.

We separate the dynamic average photon density and carrier concentration by writing the local photon density and carrier

concentration as

$$P(z,t) = \bar{P}(t)(1+f(z)) \tag{14a}$$
$$N_P(z,t) = N_P(t) + \delta N(t) f(z) \tag{14b}$$

where $\delta N \ll N_P$, $f(z)$ being a function that is smaller than unity and for which

$$\int_0^L f(z)\,dz = 0 \tag{15}$$

where L is the cavity length. Substituting (14) into (13) and ignoring the effective gain compression factor in (13), as the gain saturation parameters ε_1 and ε_2 due to the lateral effects have less influence on the damping rate of lasers, we obtain

$$\frac{d\bar{P}}{dt} = \left(\Gamma_x(\Gamma_{y1}G_P(N_P) + \Gamma_{y2}v_g a_N \delta N) - v_g\alpha_p'\right)\bar{P} \tag{16a}$$
$$\frac{dN_p}{dt} = \frac{J}{qd} - \frac{N_p}{\tau} - (\Gamma_{y1}G_P(N_P) + \Gamma_{y2}v_g a_N \delta N)\bar{P}. \tag{16b}$$

δN can be approximated by steady-state consideration [5] and is given by

$$\delta N = -\tau v_g a_N \Gamma_{y2}\bar{P}/\eta(1+\chi_3\bar{P}) \tag{17}$$

where $\chi_3 = \tau v_g a_N \Gamma_{y3}/\eta$, $\Gamma_{y1}(=\bar{\Gamma}_y + \Gamma_{Lp})$, Γ_{y2}, and Γ_{y3} are defined as first-, second-, and third-order lateral confinement factors, $\alpha_p'(=\alpha_s+\alpha_{Lp})$ is the equivalent cavity loss, and η is a normalizing factor. Their definitions are given in Appendix B.

Using small-signal analysis technique, the relaxation oscillation frequency ω_f of the DTWG-DFB lasers can be deduced and is given by

$$\omega_f^2 = v_g^2 a_N \Gamma_{y1}\bar{P}_0\alpha_p'\left(1 + 2(\chi_3 - \chi_4)\bar{P}_0 - 3\chi_3\chi_4\bar{P}_0^2\right)$$
$$\approx v_g^2 a_N \Gamma_{y1}\bar{P}_0\alpha_p' \tag{18}$$

where $\bar{P}_0$ is the steady-state photon density and $\chi_4 = \chi_3 + \tau v_g a_N \Gamma_{y2}^2/\Gamma_{y1}\eta$. The influence of gain saturation due to longitudinal SHB of carrier concentration (i.e., χ_3 and χ_4) is ignored in (18).

In the derivation of (18), the influence of gain compression due to combined lateral and longitudinal effects has been ignored and this assumption will be verified in the following numerical analysis. On the other hand, the simplified expression of ω_f shows some important insights into how the tapered waveguide structure influences the relaxation oscillation frequency of DTWG-DFB lasers. As we can see, the first-order lateral confinement factor Γ_{y1} is defined as the sum of $\bar{\Gamma}_y$ (i.e., average value of Γ_y) and Γ_{Lp} (i.e., the overlapping integral of $f(z)$ and Γ_y). The equivalent cavity loss α_p' is equal to the sum of α_s (i.e., cavity loss) and α_{Lp} (i.e., the overlapping integral of $\alpha_p(z)$ and $f(z)$) (see Appendix B). These indicate that the terms $\bar{\Gamma}_y$, Γ_{Lp}, α_s, and α_{Lp} should be optimized in order to enhance the value of ω_f.

The possibilities to maximize the value of ω_f are discussed as follows.

1) In order to maximize the value of $\bar{\Gamma}_y$, a wide stripe-width design should be adopted provided that the suppression of high-order lateral modes can be maintained by the diffraction effects of the DTWG structure.
2) It is assumed that α_s is uniform along the active and blocking regions such that its magnitude will not be affected by the laser structure.
3) A positive value of Γ_{Lp} with maximum magnitude can be obtained if the longitudinal distribution of Γ_y and the function $f(z)$ are matched. It must be noted that the longitudinal profile of Γ_y is mainly determined by the waveguide design; however, the longitudinal distribution of $f(z)$ is affected by the waveguide design as well as the κL of the lasers. In order to maximize the value of Γ_{Lp}, the profile of $f(z)$ should be selected to match with Γ_y.
4) In order to maximize the overlapping integral α_{Lp}, it is required to study the relation between $\partial|F|^2 - |R|^2/\partial z(\equiv q(z))$ and $f(z)$. It is expected that the longitudinal distribution function $q(z)$ is affected by the waveguide design as well as the κL of the lasers. On the other hand, for devices with symmetric waveguide structure, it can be shown that the function $q(z)$ has a symmetric distribution profile and its shape is close to the longitudinal distribution of carrier concentration. Let's consider the laser with symmetric waveguide structure such that we can write

$$|F(z)|^2 + |R(z)|^2 = |F(z)|^2 + |F(L-z)|^2 \tag{19a}$$

and let $\partial|F(z)|^2/\partial z = |G(z)|^2$. Then the function $q(z)$ can be rewritten as

$$\begin{aligned} q(z) &= \partial|F(z)|^2 - |R(z)|^2/\partial z \\ &= \partial|F(z)|^2 - |F(L-z)|^2/\partial z \\ &= |G(z)|^2 + |G(z-L)|^2. \end{aligned} \tag{19b}$$

Hence, the longitudinal profile of $q(z)$ is inversely proportional to the longitudinal distribution of photon density (as well as $f(z)$) due to the partial differentiation terms. Therefore, the overlapping integral of α_{Lp} may give a negative value and is minimized for high κL devices because high κL devices accumulate more photon energy inside the cavity than low κL devices (i.e., severe longitudinal SHB for high κL devices).
5) It has been shown that high κL devices have relatively high ω_f. This is because the total energy stored inside the laser cavity, which is proportional to ω_f, is high for high κL devices [4]. Therefore, we expect ω_f of DTWG-DFB lasers increases with κL.

From the above prediction on the dynamic behavior of DTWG-DFB lasers, it is shown that ω_f in general increases with stripe width and κL; however, the variation of Γ_{Lp} and α_{Lp} may work against the change of ω_f. In the following numerical analysis, we study the influence of stripe width and κL on the variation of ω_f and the overlapping integrals (i.e., Γ_{Lp} and α_{Lp}) separately.

III. Simulation Results

A. DTWG-DFB Lasers: Structure and Material Composition

The waveguide structure and the material composition of the lasers used in this paper are similar to that given in [2].

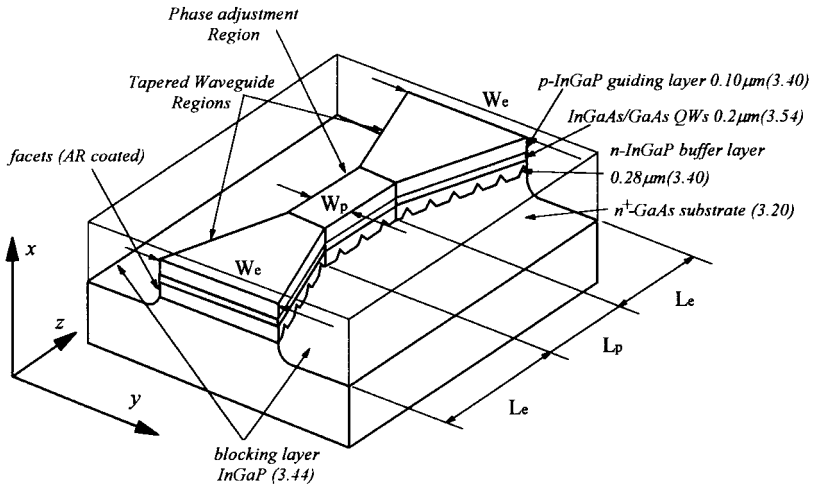

Fig. 1. Schematic of a buried structure DFB laser with double-tapered-waveguide structure.

TABLE I
DEVICE PARAMETERS USED IN THE MODEL

Parameters (symbol)	Magnitude
Carrier lifetime (τ)	3×10^{-9}s
Differential gain (a_N)	3×10^{-16}cm^2
Transparency carrier density(N_o)	1.5×10^{18}cm^{-3}
Linewidth enhancement factor (α_m)	3.0
Absorption and scattering loss (α_s)	40cm^{-1}
Effective group refractive index (n_g)	3.70
Thickness of the active layer (d)	0.2μm
Approximate emission wavelength (λ_o)	0.98μm
Transverse optical confinement factor (Γ_x)	0.35
Period of grating (Λ)	0.145μm
Group velocity (v_g)	8×10^9cm/s
magnitude of Left facet reflectivity ($\|r_L\|$)	0
magnitude of Right facet reflectivity ($\|r_R\|$)	0

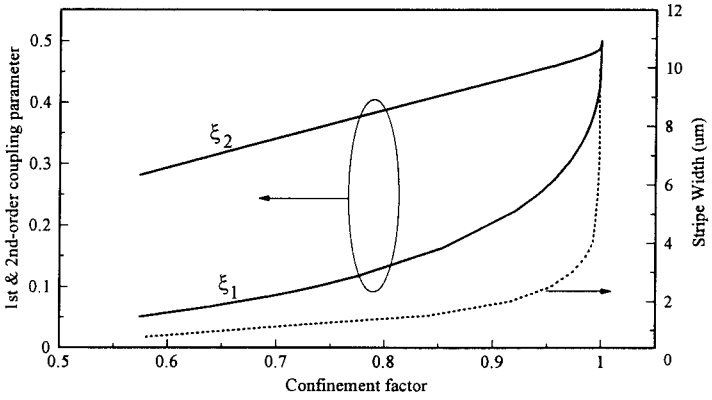

Fig. 2. The variation of stripe width, first-order ξ_1 and second-order ξ_2 coupling parameters with the lateral confinement factor Γ_y.

It is assumed that the waveguide geometry has a double-tapered structure with a phase-adjustment region (PAR) in between (see Fig. 1). The laser is composed of five layers of semiconductor materials: the p$^+$-GaAs cladding layer, p-InGaP guiding layer, the InGaAs–GaAs (0.98 μm) quantum well's active region, the n-InGaP buffer layer and n$^+$-GaAs substrate. The BH is used to provide strong optical and electrical confinement along the lateral direction. Device parameters used in the model can be found in Table I.

In the following sections, it is assumed that the lasers have symmetric waveguide geometry with both facets antireflection-coated. The width of the PAR W_p and the tapered waveguide near facets W_e varies from 1 to 2 μm and from 2 to 6 μm, respectively. The corresponding length of the tapered section L_e is equal to 135 μm and that of PAR L_p is equal to 110 μm such that single-mode operation can be maintained. For the reason of comparison, the steady-state photon density at the facets is set to be around 2×10^{14} cm^{-3}.

B. Relaxation Oscillation Frequency of DTWG-DFB Lasers: Numerical Analysis

In the numerical analysis of BH-DFB lasers given in [4], it is shown that the magnitude of ω_f is affected by the magnitude of Γ_y, ξ_1, and ξ_2, especially for Γ_y, ξ_1, and ξ_2 approach their limited values (i.e., $\Gamma_y \rightarrow 1.00$, $\xi_1 \rightarrow 0.50$, $\xi_2 \rightarrow 0.50$). In DTWG-DFB lasers, these parameters are varied along the laser waveguide. Fig. 2 shows the general plot of ξ_1 and ξ_2 against Γ_y for a strong index-guided waveguide. The corresponding variation of stripe width with Γ_y is also shown in the diagram. As we can see for the stripe width larger than or equal to 4 μm, the magnitude of Γ_y, ξ_1, and ξ_2 approach their limited values. In the following paragraphs, the influence of Γ_y, ξ_1, and ξ_2 (due to the longitudinal variation of stripe width) on the dynamic behavior of DTWG-DFB lasers is analyzed numerically.

Fig. 3 shows the variation of ω_f^2 as a function of W_e for devices with $D_f = 5$ cm^{2}s^{-1} and κ_o =30, 50, and 80 cm^{-1}. As we can see, ω_f^2 increases with W_e and is high for the device with $W_p = 2$ μm and $\kappa_o = 80$ cm^{-1}. The influence of W_e on the transient response of the output power for device with $W_p = 2$ μm, $D_f = 5$ cm^{2}s^{-1} and $\kappa_o = 50$ cm^{-1} is shown in Fig. 4. The damping rate for devices with $W_e = 2$ and 5 μm exhibit similar magnitude such that our assumption used in the derivation of (16) (i.e., ignorance of gain compression due to lateral effects) is satisfied.

The influence of D_f on ω_f^2 of DTWG-DFB lasers with $\kappa_o =$ 50 cm^{-1} is shown in Fig. 5. As we can see, ω_f^2 increases with D_f from 0 to 5 cm^2·s^{-1} and is saturated for $D_f \geq 5$ cm^2·s^{-1}.

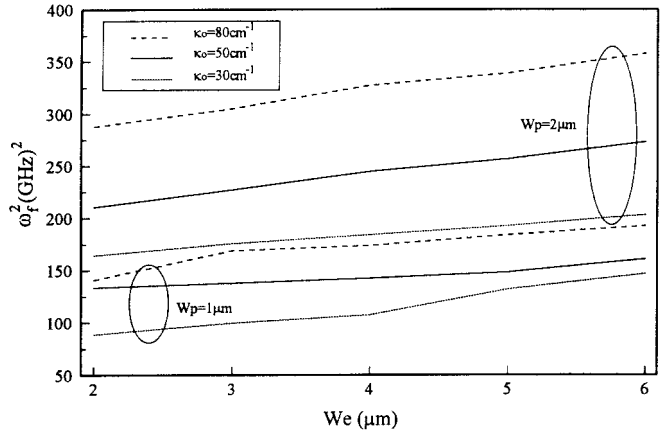

Fig. 3. The variation of ω_f^2 with W_e for lasers with $D_f = 5$ cm^2·s^{-1}, $W_p = 1$ and 2 μm, $\kappa_o = 30$ cm^{-1} (dotted line), $\kappa_o = 50$ cm^{-1} (solid line) and $\kappa_o = 80$ cm^{-1} (dashed line).

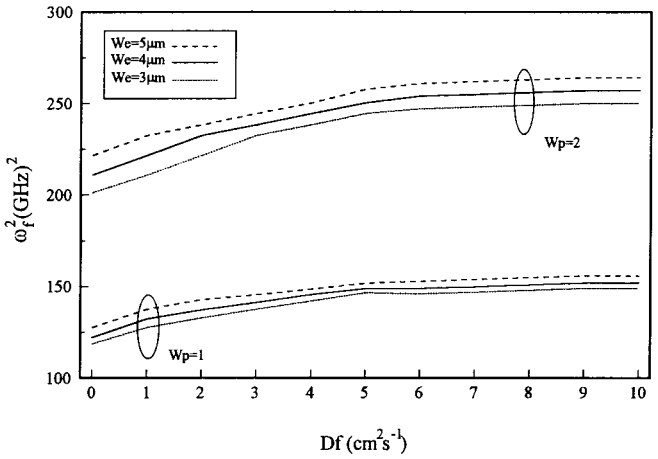

Fig. 5. The variation of ω_f^2 with D_f for lasers with $\kappa_o = 50$ cm^{-1}, $W_p = 1$ and 2 μm, $W_e = 3$ μm (dotted line), $W_e = 4$ μm (solid line), and $W_e = 5$ μm (dashed line).

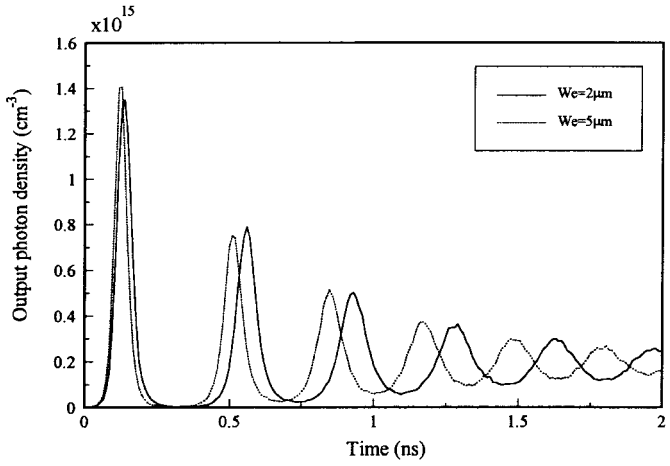

Fig. 4. Transient response of the output photon density for devices with $W_e = 2$ and 5 μm. The other parameters are $D_f = 5$ cm^2·s^{-1}, $\kappa_o = 50$ cm^{-1} and $W_p = 2$ μm.

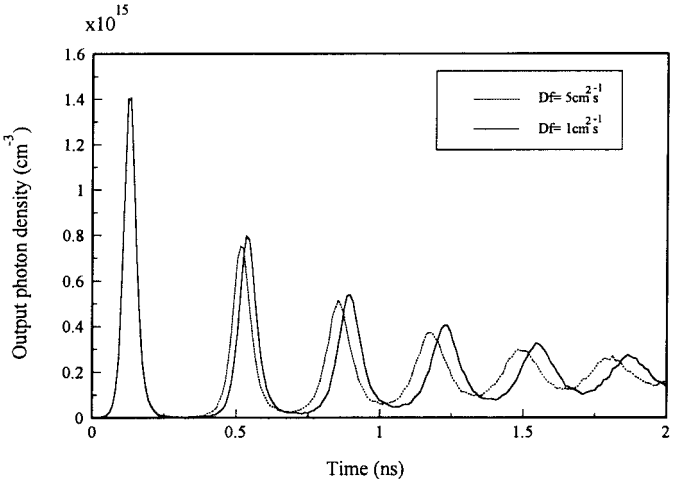

Fig. 6. Transient response of the output optical photon density for devices with $D_f = 1$ and 5 cm^2·s^{-1}. The other parameters are $W_e = 5$ μm, $\kappa_o = 50$ cm^{-1}, and $W_p = 2$ μm.

The magnitude of ω_f^2 remains unchanged for further increase of D_f to 50 cm^2·s^{-1}. The influence of D_f on the transient response of the output power for devices with $W_p = 2$ μm, $W_e = 5$ cm^2·s^{-1} and $\kappa_o = 50$ cm^{-1} is also shown in Fig. 6. As we can see, the lateral carrier diffusion has less influence on the damping rate of the devices.

The dynamic behavior of DTWG-DFB lasers can be summarized as follows.

1) ω_f increases with W_e and W_p. This is because the increase of W_e and W_p increases the value of Γ_y, ξ_1, and ξ_2 (i.e., this is equivalent to increasing the value of $\bar{\Gamma}_y$).
2) ω_f is saturated at a high magnitude for $D_f \geq 5$ cm^{2}s^{-1} and this characteristic is different to uniform-stripe BH-DFB lasers [4].
3) W_e, W_p, and D_f have less influence on the damping rate of DTWG-DFB lasers and this implies that the induced gain compression due to lateral effects can be ignored in our analysis.
4) ω_f increases with κ_o; however, κ_o has less influence on the damping rate of the lasers. This indicates that the induced gain compression due to longitudinal SHB has less contribution on the dynamic behavior of the devices.

The numerical results show that ω_f increases with stripe width (i.e., W_e and W_p) and κL, which partly verifies our analytical prediction on the dynamic behavior of DTWG-DFB lasers. Now, we further investigate the relation between the overlapping integrals (i.e., Γ_{Lp} and α_{Lp}) and the devices' parameters (i.e., W_e, W_p, and κL).

It is assumed in this study that devices have $W_p = 2$ μm and $D_f = 5$ cm^2·s^{-1}. As shown in Fig. 7, Γ_y exhibits a "U" shape with minimum at the PAR and maximum near the facets. Γ_y approaches its limited value (i.e., $\Gamma_y \approx 1.00$ near the facets region) as W_e approaches 4 μm. The function $f(z)$ defined in (14) can be obtained from the longitudinal distribution of optical density

$$f(z) = \left(|F(z)|^2 + |R(z)|^2\right)/\bar{P}_0 - 1. \qquad (20)$$

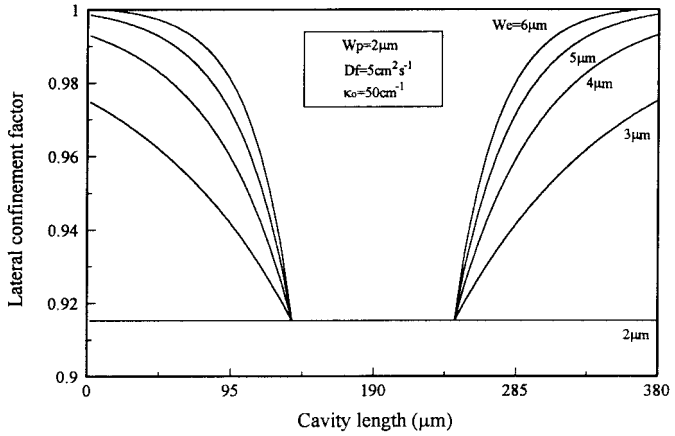

Fig. 7. The variation longitudinal distribution of lateral confinement factor Γ_y with W_e. The other parameters are $D_f = 5$ cm^2·s^{-1}, $\kappa_o = 50$ cm^{-1}, and $W_p = 2$ μm.

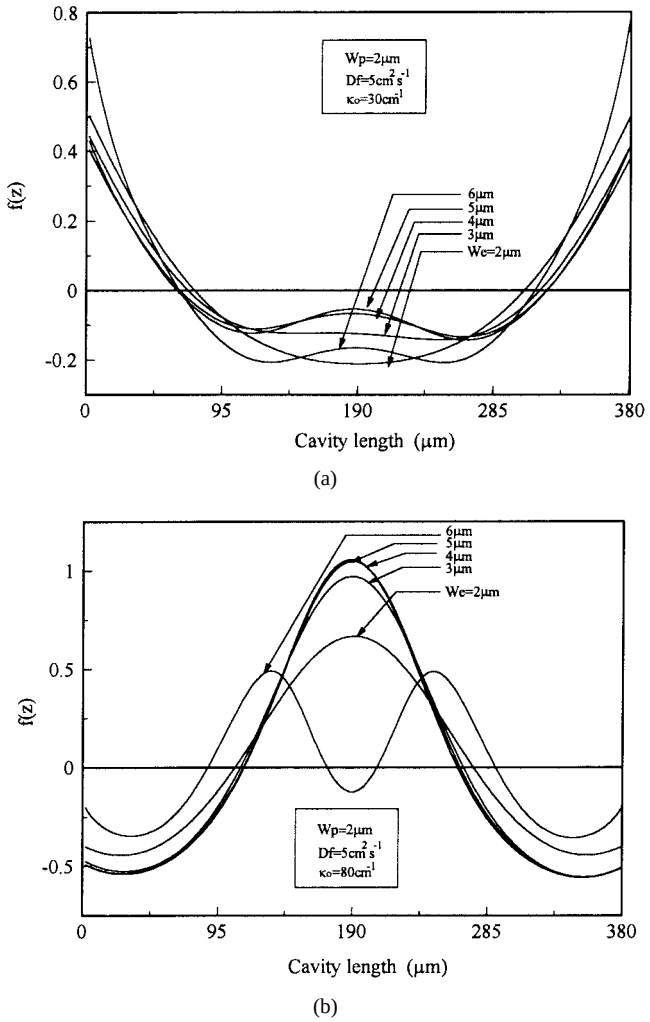

Fig. 8. The variation of $f(z)$ with W_e for devices with (a) $\kappa_o = 30$ cm^{-1} and (b) $\kappa_o = 80$ cm^{-1}. The other parameters are $D_f = 5$ cm^2·s^{-1} and $W_p = 2$ μm.

Fig. 8 plots the longitudinal distribution of $f(z)$ for devices with $\kappa_o = 30$ and 80 cm^{-1} for a range of W_e. As we can see, the profile of $f(z)$ is close to Γ_y for a device with $\kappa_o = 30$ cm^{-1} but is convex upwards near the PAR for a device with $\kappa_o \geq 50$ cm^{-1} which is totally mismatched with the profile of Γ_y. Therefore, it is expected that the value of Γ_{Lp} can be enhanced for $\kappa_o \leq 30$ cm^{-1} due to matching of the longitudinal profile of $f(z)$ and $\Gamma_y(z)$. The longitudinal distribution of $q(z)$ for $W_e = 5$ μm is also shown in Fig. 9. It is shown that the longitudinal distribution of $q(z)$ is inversely proportional to the profile of $f(z)$. The corresponding variation of Γ_{Lp} and α_{Lp} with W_e is shown in Fig. 10. As we expected, the value of Γ_{Lp} and α_{Lp} decreases with the increase of W_e for devices with $\kappa_o \geq 50$ cm^{-1}. This is because: 1) the "U" shape profile of Γ_y is mismatched with the $f(z)$ which is convex upwards near the PAR and hence the value of Γ_{Lp} is reduced; 2) $f(z)$ is more convex upwards with the increase of W_e and κ_o such that the value of α_{Lp} is reduced. We can conclude that Γ_{Lp} and α_{Lp} are reduced with the increase of W_e and κ_o due to the longitudinal SHB which may reduce the value of ω_f. However, from our numerical study on ω_f, it is shown that ω_f increases with W_e and κ_o which indicates that the effects of Γ_{Lp} and α_{Lp} have been overcome by $\bar{\Gamma}_y$ and total energy stored inside the laser cavity.

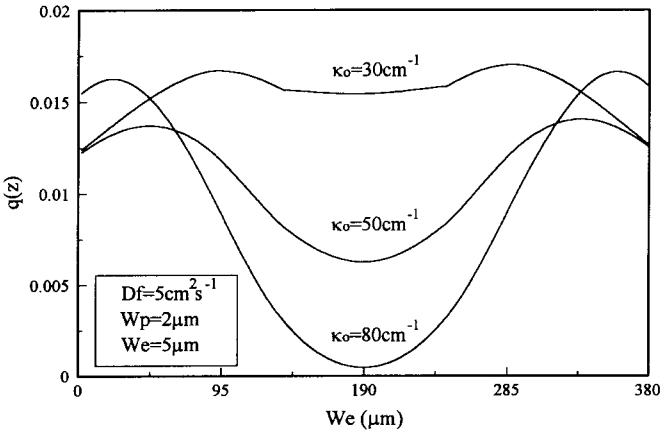

Fig. 9. The longitudinal variation of $q(z)$ with κ_o. The other parameters are $D_f = 5$ cm^2·s^{-1}, $W_e = 5$ μm, and $W_p = 2$ μm.

IV. Conclusion

The influence of a DTWG structure on ω_f of DFB lasers is clarified. By using the first-order approximation on the combined lateral and longitudinal distribution of carrier concentration, the ω_f of DTWG-DFB lasers is deduced analytically. It is illustrated from (18) that the longitudinal SHB reduces ω_f through the terms Γ_{Lp} and α_{Lp}. Γ_{Lp} is arisen from the DTWG structure and α_{Lp} is an inherent property of DFB lasers. However, ω_f is an increasing function of stripe width because the influence of SHB is overcome by $\bar{\Gamma}_y$. In addition, ω_f is increased with κL as well as the total energy stored inside the laser cavity. Hence, the value of ω_f can be enhanced for devices with wide stripe width and high κL.

Our analytical analysis on ω_f is also verified by our numerical results. It is found that the combined longitudinal and lateral effects have less influence on the damping rate of the lasers. Hence, the ignorance of the effective gain compression factors due to the combined longitudinal and lateral effects in the derivation of ω_f in Section II-B is satisfied.

In the design of DTWG-DFB lasers, a wide tapered region and high κL are required to enhance ω_f provided that

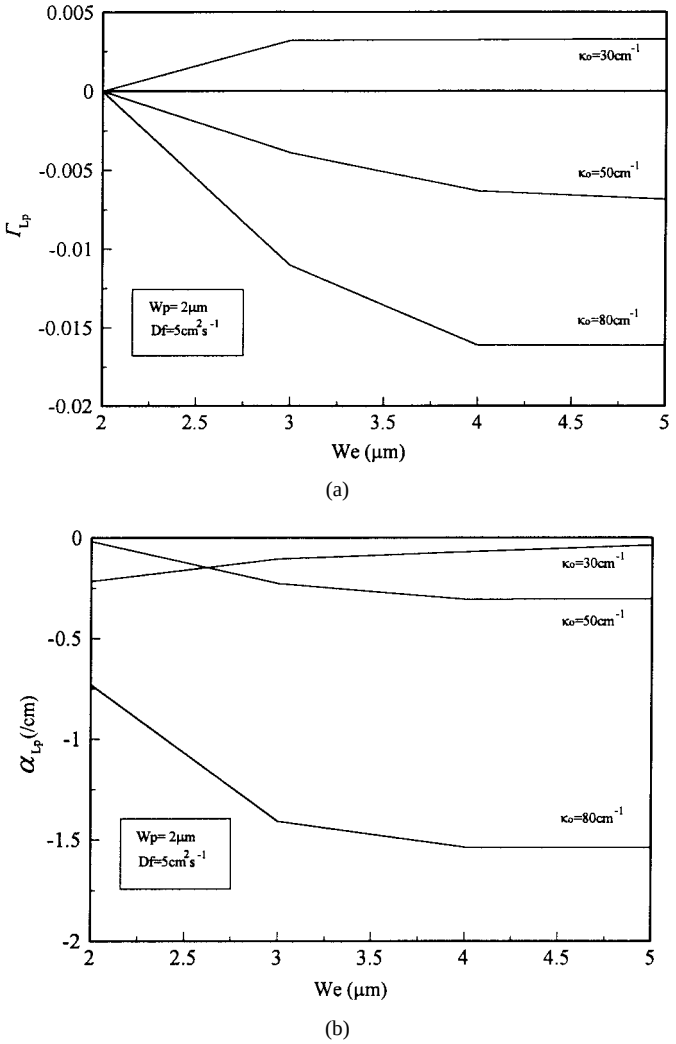

Fig. 10. The variation of (a) the overlapping integral Γ_{Lp} and (b) the overlapping integral α_{Lp} for devices with κ_o = 30–80 cm^{-1} and W_e = 2–5 μm.

single-lateral-mode operation can still be maintained by the diffraction effects of the DTWG structure. Therefore, the DTWG structure gives a simple solution to maintain high ω_f and stable lateral mode operation, and this is the major advantage over the uniform stripe devices. This is because in order to enhance ω_f in uniform stripe BH-DFB lasers, it may require increasing the stripe width (i.e., Γ_y changes from $\sim$0.7 to $\sim$1.0) which will also excite high-order lateral modes.

The dynamic behavior of DTWG-DFB lasers is analyzed theoretically. It is shown that the modulation bandwidth DFB lasers, especially for large κL, can be enhanced with a DTWG structure. Apart from stable-single-mode and high power characteristics, DTWG-DFB lasers also have significant improvement in modulation speed over the conventional uniform stripe devices.

Appendix A

We assumed the field profiles in the transverse (x) and lateral (y) directions satisfy [7]

$$\left[\frac{\partial^2}{\partial x^2} + \varepsilon_{\text{eff}} k_o^2 - \beta_{\text{eff}}^2\right]\phi_o = 0 \tag{A1}$$

$$\left[\frac{\partial^2}{\partial y^2} + \left(\beta_{\text{eff}}^2 - \beta^2\right)\right]\psi_o = 0 \tag{A2}$$

where β_{eff} is the effective propagation coefficient in lateral direction and β is a propagation constant to be determined. ϕ_o and ψ_o are the fundamental transverse and lateral field distributions, respectively. ε_f is the effective permittivity and is given by [8]

$$\begin{aligned}\varepsilon_f(y,z,t) &= n_a^2(y) - n_a(y)\Gamma_x \frac{\alpha_m \lambda_o}{2\pi} a_N(N(y,z,t) - N_{\text{th}}) \\ &\quad + i\frac{\lambda_o n_a(y)}{2\pi}\Gamma_x[a_N(N(y,z,t) - N_o) - \alpha_s]\end{aligned} \tag{A3}$$

where n_a is the built-in refractive index of the waveguide, α_m is the material linewidth enhancement factor, and N_{th} is the threshold carrier concentration.

The effective refractive index n_{eff} given in (3) is defined as [7]

$$n_{\text{eff}} = \beta_{\text{eff}}/k_o \tag{A4}$$

where $k_o = 2\pi/\lambda_o$. The transverse confinement factor Γ_x is expressed as

$$\Gamma_x = \int\limits_{\substack{\text{active}\\ \text{layer}}} \phi_o^2 \, dx \tag{A5}$$

and the lateral confinement factor Γ_y is given by

$$\Gamma_y = \int_0^w \psi_o^2 \, dy \tag{A6}$$

where w is the width of waveguide. The longitudinal coupling coefficient κ is given by

$$\kappa = \frac{1}{2\beta_o}\int_0^w \int\limits_{\substack{\text{grating}\\ \text{layer}}} k_o^2 A_{-2}\phi_o^2\psi_o^2 \, dx\, dy \approx \kappa_o \Gamma_y \tag{A7}$$

where A_{-2} is the Fourier coefficient of the dielectric grating, β_o is the propagation constant at Bragg frequency, and κ_o is the coupling coefficient of PAR.

The first- and second-order coupling parameters are given by

$$\xi_1 = \int_{-w/2}^{w/2} \cos(2\pi y/w)\psi_o^2(y)\, dy \tag{A8}$$

$$\xi_2 = \int_{-w/2}^{w/2} \cos^2(2\pi y/w)\psi_o^2(y)\, dy. \tag{A9}$$

Appendix B

The first-, second-, and third-order lateral confinement factor Γ_{y1}, Γ_{y2}, and Γ_{y3} are given by

$$\Gamma_{y1} = \frac{1}{L}\int_0^L \Gamma_y(z)(1 + f(z))\, dz = \bar{\Gamma}_y + \Gamma_{Lp} \tag{B1}$$

$$\Gamma_{y2} = \frac{1}{L}\int_0^L \Gamma_y(z) f(z)(1 + f(z))\, dz \tag{B2}$$

$$\Gamma_{y3} = \frac{1}{L}\int_0^L \Gamma_y(z) f^2(z)(1 + f(z))\, dz \tag{B3}$$

where $\bar{\Gamma}_y = \frac{1}{L}\int_0^L \Gamma(z)\,dz$ is the average value of of $\Gamma_y(z)$ and $\Gamma_{Lp} = \frac{1}{L}\int_0^L \Gamma_y(z)f(z)\,dz$ is the overlapping integral of $\Gamma_y(z)$ and $f(z)$.

The equivalent cavity loss α_p' is given by

$$\alpha_p' = \frac{1}{L}\int_0^L \alpha_p(z)(1+f(z))\,dz = \alpha_s + \alpha_{Lp} \tag{B4}$$

where α_{Lp} is given by

$$\begin{aligned}\alpha_{Lp} &= \frac{1}{L}\int_0^L \frac{1}{|F|^2+|R|^2}\left(\frac{\partial}{\partial z}|F|^2 - |R|^2\right)f(z)\,dz \\ &= \frac{1}{P_0 L}\int_0^L \frac{1}{(1+f(z))}\left(\frac{\partial}{\partial z}|F|^2 - |R|^2\right)f(z)\,dz. \end{aligned}\tag{B5}$$

The normalization factor η is equal to

$$\eta = \frac{1}{L}\int_0^L f^2(z)\,dz. \tag{B6}$$

REFERENCES

[1] S. F. Yu, "Quasi 3-dimensional large signal dynamic model of DFB lasers," *IEEE J. Quantum Electron.*, vol. 32, pp. 424–432, Mar. 1996.

[2] ——, "Double tapered waveguide distributed feedback lasers for high power single mode operation," *IEEE J. Quantum Electron.*, vol. 33, pp. 71–80, Jan. 1997.

[3] S. F. Yu and E. H. Li, "Influence of lateral field on the relaxation oscillation frequency of semiconductor lasers," *IEEE J. Quantum Electron.*, vol. 32, pp. 1–3, Jan. 1996.

[4] S. F. Yu, R. G. S. Plumb, L. M. Zhang, M. C. Nowell, and J. E. Carroll, "Large signal dynamic behavior of distributed feedback lasers including lateral effects," *IEEE J. Quantum Electron.*, vol. 30, pp. 1740–1750, Aug. 1994.

[5] G. Morthier, F. Libbrecht, K. David, P. Vankwikelberge, and R. G. Baets, "Theoretical investigation of the second-order harmonic distortion in the AM response of 1.55 μm F-P and DFB lasers," *IEEE J. Quantum Electron.*, vol. 27, pp. 1990–2002, 1991.

[6] P. Vankwikelberge, F. Buytaert, A. Franchois, R. Baets, P. I. Kuindersma, and C. W. Fredriksz, "Analysis of the carrier-induced FM response of DFB lasers: Theoretical and experimental case studies," *IEEE J. Quantum Electron.*, vol. 25, pp. 2239–2254, 1989.

[7] M. J. Adams, *An Introduction to Optical Waveguides*. New York: Wiley, ch. 6.

[8] S. F. Yu and E. H. Li, "The effects of lateral modes on static and dynamic behavior of buried heterostructure DFB lasers," in *Proc. Inst. Elect. Eng., Optoelectronics*, vol. 142, pt. J, no. 2, pp. 97–102, 1995.

[9] R. Tucker and D. J. Pope, "Circuit modeling of diffusion on damping in a narrow-stripe semiconductor laser," *IEEE J. Quantum Electron.*, vol. QE-19, pp. 1179–1183, 1983.

S. F. Yu, for photograph and biography, see p. 1008 of the June 1997 issue of this JOURNAL.